ABSTRACTS 5th WORKSHOP TURKEY, 1-2 April, 2004
Fundamental modelling of the design and performance of concrete pavements

Key-note speaker
Bridging the gap between theoretical modelling and every day practice.
Setting the scene for the 5th workshop

Dr. Raymond S. Rollings, Research Engineer, 72 Lyme Road, Hanover, USA
Theoretical Design: Still a Quantum Leap Forward

Theme
I. Fundamental modelling of material properties
- Prediction of behaviour of green concrete, based on concrete's maturity (regarding time of saw cutting, curing period, opening to heavy traffic etc.)
- Mechanical material characterisation of concrete
- High-tech cementitious materials for pavements and railway structures(new concrete mixes)

Dr. D. Zollinger and Jin-Hoon Jeong, Texas A&M University USA
Environmental effects on the behavior of jointed plain concrete pavements

Ru Mu, Klaas van Breugel, Faculty of Civil Engineering and Geosciences, Delft University of Technology, Stevinweg 1 2628 CN, Delft, the Netherlands
Microcracking and Surface Scaling of Air-Entrained SFRC Pavements Subjected to Simultaneous Action of Flexural Load and Freeze-Thaw cycles

Dipl.-Ing. M. Sule, Dr. ir. C van der Veen, Prof.dr.ir. K. van Breugel
Delft University of Technology, The Netherlands
Development of bond between reinforcement steel and early-age concrete

Dr. Anton Schindler, Harbert Engineering Center, Auburn University, Alabama, U.S.A
Prediction of Concrete Setting

Theme:
II. Theoretical models
- Multilayer versus plate model
- Finite Element Modelling
- Crack models for continuous reinforced concrete pavement (load and deformation controlled)
- Effects of thermal and moisture gradients on internal deformations / stresses
- Probabilistic design or risk analysis
- Design and evaluation of concrete pavements

Prof. Johan Silfwerbrand, Swedish Cement and Concrete Research Institute, Stockholm, Sweden
Curling of New-cast Concrete Pavements – A Theoretical Discussion

C.R. Braam, Delft University of Technology, Concrete Structures Group, The Netherlands
J.W. Frénay, ENCI bv, 's-Hertogenbosch, The Netherlands
Controlled cracking of continuous reinforced concrete pavements: theory and verification of in-situ measurements

Anastasios (Tasos) M. Ioannides & J. Peng, University of Cincinnati, Cincinnati, OH, USA
Finite element simulation of crack growth in pcc slabs: implications for concrete pavement design

Marc Stet and Frans Van Cauwelaert, KOAC WMD Apeldoorn, The Netherlands
The elastic length: key to the analysis of multilayered concrete structures

Ph.D. Ali A. Farhang, ELU Consult AB, Danderyd, Sweden
Calculation of Thermal Stresses for Jointed Plain Concrete Pavements Based on Non-linear Temperature Gradients Using Modified *Eisenmann`s* Equation and Modified *Silfwerbrand`s* Plate Method

Dr. Lev Khazanovich, University of Minnesota, Minneapolis, USA
Curling analysis of slabs on pasternak foundation

Ir M. Lemlin, MET
Ir D. Leonard, BRRC
Ir A. Jasienski, FEBELCEM, BELGIUM
Dr Ir F. Van Cauwelaert
The computation of thermal stresses in layered concrete structures on a Pasternak foundation

Dr. Lee York Ying-Haur, Tamkang University, Ying-Chuan Rd., Tamsui, Taipei, Taiwan
Parameter Studies and Verifications on Three-Dimensional Finite Element Analysis of Rigid Pavements

Doctor Armelle Chabot & P. Tamagny, LCPC, Centre de Nantes, Bouguenais Cedex, France
Q.D. Tran & A. Ehrlacher, ENPC, Marne la Vallée, France
Stress Fields Modelling for Cracking in Pavements

Ir. A.C. Pronk, RWS-DWW, Delft, The Netherlands
Corner Loading "The final quest"

Dr. Halil Ceylan, Iowa State University of Science and Technology and Dr. Erol Tutumluer and Dr. Ernest J. Barenberg, University of Illinois at Urbana-Champaign, USA
Use of Artificial Neural Networks for the Analysis & Design of Concrete Pavement Systems

Guido Bonin, Giuseppe Cantisani, Giuseppe Loprencipe and Alessandro Ranzo, Dipartimento di Idraulica, Trasporti e Strade (DITS), Università degli Studi di Roma "La Sapienza", Italy

Modeling of dynamic phenomena in road and airport pavements

L. Heleven, LIN Afdeling Wegenbouwkunde, P. Bumma, MET Direction des Structures routières, Dr. Ir. F. Van Cauwelaert, Belgium
Evaluation of continuously reinforced concrete pavements in Belgium

Theme

III. Theoretical models related to pavement performance

- Performance modelling (cracking, visual condition)
- Pavement test tracks in laboratory and on the road

Julie M. Vandenbossche, P.E., Assistant Professor, University of Pittsburgh, USA
Mark B. Snyder, Ph.D, P.E., Executive Director, Minnesota Concrete Paving Association, Minnesota, USA
Interpreting the Effects of Curled/Warped Pavements on the Analysis of FWD Data

Thomas D. White, Mississippi State University, Mississippi State, Mississippi, USA
Sameh M. Zaghloul, Stantec, Kitchener, Ontario, Canada
Response Based Load Equivalencies for Concrete Pavements

Michael Darter, ERES Division of ARA, Inc, USA
Design of Concrete Pavement Using Incremental Damage Approach

Dr. Tatsuo Nishizawa, Ishikawa National College of Technology and Yasushi Takeuchi and Masashi Koyanagawa, Tokyo University of Agriculture, Japan
Effects of Plastic Deformation of Granular Base on Performance of Concrete Pavement Slab

Dr. Juan Pablo Covarrubias, Instituto del Cemento y del Hormigón de Chile (ICH), Chile
Concrete pavement performance models in HDM4

Shiraz D. Tayabji, Ph.D., P.E, Construction Technology Laboratories, Inc, USA
Determination of optimum lane width for widened lane concrete pavements

Theme:

IV. Design of innovative pavement applications

- Ballast less railway tracks (slabtrack)
- Theoretical aspects of fast track paving techniques
- Detailing of CRCP (joints, pavement end parts)
- Thin concrete inlays / overlays / ultra thin white topping
- Prevention of reflective cracking from cement bound base courses

C.R. Braam, Delft University of Technology, Concrete Structures Group, The Netherlands
P. Buitelaar, Contec ApS, Højbjerg, Denmark
N. Kaptijn, Ministry of Transport, Public Works and Water Management, Structural Development Department, Tilburg, The Netherlands
Reinforced high performance concrete overlay system for steel bridges

José T. Balbo & Deividi S. Pereira & A. A. Severi, University of São Paulo, Brazil
Field responses of ultrathin whitetopping instrumented sections

Dr. P. Strauss, PO Box 588, La Montagne, South Africa
B. Perrie, Cement & Concrete Institute, South Africa
A critical thickness for thin concrete pavements

Ir. L.J.M. Houben and dr.ir. M. Huurman, Delft University of Technology, Delft, The Netherlands
S. Poot, Modieslab v.o.f., Son, The Netherlands
J. van der Kooij, Ministry of Transport, Public Works and Water Management, Road and Hydraulic Engineering Division, Delft, The Netherlands
Accelerated Load Testing and Modelling of 'Modieslab' concrete pavement structure

Prof. dr. ing. Gunther Leykauf, Munich University of Technology, Munich, Germany
Co-authors: Freudenstein S, Lechner B.
Joint effectiveness problems on floating slab tracks

Parameter Studies on Three-Dimensional Finite Element Analysis of Rigid Pavements

Ying-Haur Lee, Hsin-Ta Wu, & Shao-Tang Yen
Department of Civil Engineering, Tamkang University, Tamsui, Taiwan

ABSTRACT: The main objective of this study was to conduct in-depth parameter studies on 3-D finite element (FE) analysis of rigid pavements under edge loading conditions. A systematic analytical approach was utilized and implemented in a Visual Basic software package to study the effects of mesh fineness and element selection. The deflection and stress convergence characteristics of various 2-D shell and 3-D solid elements were investigated. Several guidelines in mesh fineness and element selection were developed and recommended. Using the principles of dimensional analysis, an additional dimensionless variable (h/a) was identified and verified to have a substantial influence on ABAQUS runs using either 2-D shell or 3-D solid elements. Separate 3-D FE stress and deflection databases were developed using all dimensionless variables. An example critical stress predictive model was developed. Together with the existing 2-D FE research findings, a tentative stress prediction equation was proposed to illustrate its possible applications.

KEY WORDS: Rigid pavement, finite element model, stress, deflection, design, evaluation.

1. INTRODUCTION

Determination of critical structural responses in terms of stresses and deflections in a concrete slab is essential to mechanistic-based design as well as structural evaluation procedures. Two-dimensional (2-D, ILLI-SLAB) finite element (FE) models have been successfully utilized to account for the effects of many practical pavement conditions more realistically than theoretical solutions based on infinite slab and full contact assumptions (Lee, 1999). The applicability of the ILLI-SLAB program for stress estimation has been previously investigated through comparisons of the resulting stresses and the actual field measurements from some test sections of Taiwan's second northern highway, the AASHO Road Test, and the Arlington Road Test with reasonably good agreements.

With the introduction of three-dimensional (3-D, ABAQUS) FE and all the promising features and results reported in the literature (Ioannides and Donnelly, 1988; Kuo, 1994; Brill, 1998; Hammons, 1998; Thompson and Navneet, 1999; Kim and Hjelmstad, 2000), its applications on pavement engineering become inevitable. Nevertheless, due to the required running-time and complexity, 3-D FE analysis cannot be easily implemented as a part of design or structural evaluation procedure. Thus, the main objective of this study is to conduct in-depth parameter studies on 3-D FE analysis of rigid pavements (Wu, 2003). A single slab resting on a Winkler foundation with edge loading conditions was considered. The ultimate goal of this study is to bridge the gap among various 2-D and 3-D FE idealizations and closed-form solutions for future development of a 3-D FE mechanistic-based design and structural evaluation procedure.

2. CLOSED-FORM SOLUTIONS AND FINITE ELEMENT IDEALIZATIONS

Based on the assumption of an infinite or semi-infinite slab over a dense liquid (Winkler) foundation, Westergaard obtained the following closed-form solutions subjected to a single edge wheel load (Ioannides, 1985):

$$\sigma_{we} = \frac{3(1+\mu)P}{\pi(3+\mu)h^2}\left[\ln\frac{Eh^3}{100ka^4} + 1.84 - \frac{4}{3}\mu + \frac{1-\mu}{2} + 1.18(1+2\mu)\frac{a}{\ell}\right] \quad (1)$$

$$\delta_{we} = \frac{\sqrt{2+1.2\mu}P}{\sqrt{Eh^3k}}\left[1 - \frac{(0.76+0.4\mu)a}{\ell}\right] \quad (2)$$

Where σ_{we} is Westergaard's closed-form edge stress solution, [FL^{-2}]; δ_{we} is the edge deflection, [L]; P is the single wheel load, [F]; h is the thickness of the slab, [L]; a is the radius of the applied load, [L]; ℓ=(E*h3/(12*(1-μ2)*k))$^{0.25}$ is the radius of relative stiffness of the slab-subgrade system [L]; k is the modulus of subgrade reaction, [FL^{-3}]; E is the concrete modulus of the slab, [FL^{-2}]; μ is the Poisson's ratio. Note that primary dimension for force is represented by [F], and length is represented by [L]. γ=0.577215664901 is Euler's constant. The analysis of finite slab length and width was not possible until the introduction of finite element (FE) models. The well-known ILLI-SLAB (2-D) and ABAQUS (3-D) FE models were selected for this study (Korovesis, 1990; Hibbitt, Karlsson, and Sorensen, 2000). Brief summary characteristics of the ILLI-SLAB finite element, 2-D shell and 3-D solid elements from the ABAQUS library including both linear and quadratic elements employing both full and reduced integration were given in the literature (Kuo, 1994; Hammons, 1998; Wu, 2003). Two types of thin shell elements (4-node, 8-node, and 9-node) are considered: those satisfy the thin shell theory (the Kirchhoff constraint) analytically and those converge to thin shell theory numerically as the thickness decreases. The selected 3-D solid (brick) elements (8-node, 20-node, and 21~27-node) include first-order (linear) and second-order (quadratic) interpolation elements. Second-order elements provide higher accuracy than first-order elements and are very effective in bending-dominated problems. Reduced integration reduces the computation time through the use of a lower-order integration to form the element stiffness. Generally speaking, the accuracy achieved with full versus reduced integration first-order elements is largely dependent on the nature of the problem. For second-order elements, reduced-integration elements generally yield more accurate results than the corresponding fully integrated elements (Hammons, 1998; Hibbitt, Karlsson, and Sorensen, 2000)

3. PARAMETER ANALYSIS AND MODEL BUILDING

3.1. Definition of mesh fineness and mesh generation

Mesh generation in the horizontal direction as shown in Figure 1 generally follows the following steps: the consideration of applicable symmetry option, generation of finer mesh at the loaded area (Zone I) and at its neighborhood area (Zone II), and progressively increasing to coarser mesh further away (Zone III) for efficiency consideration. Horizontal mesh fineness is defined as the ratio of the length of the loaded area to the selected element length throughout this study. In addition, Zone I and Zone II was chosen to have the same mesh fineness, whereas the mesh of Zone III was decided as 4 times coarser than Zone I according to previous literature. The length of neighborhood area (nC) will be further investigated, though it was usually selected as 2 times the length of the loaded area (C). Although there are some controversies regarding the mesh generation in the vertical direction (Ioannides 1984; Ioannides and Donnelly, 1988; Kuo, 1994; Hammons, 1998), vast amount of computer

resources are required if a certain aspect ratio in the vertical direction is chosen especially for a small wheel load area and/or small horizontal mesh length. Thus, it was decided that vertical mesh fineness be defined as the number of evenly divided layers for practical model building concern in this study.

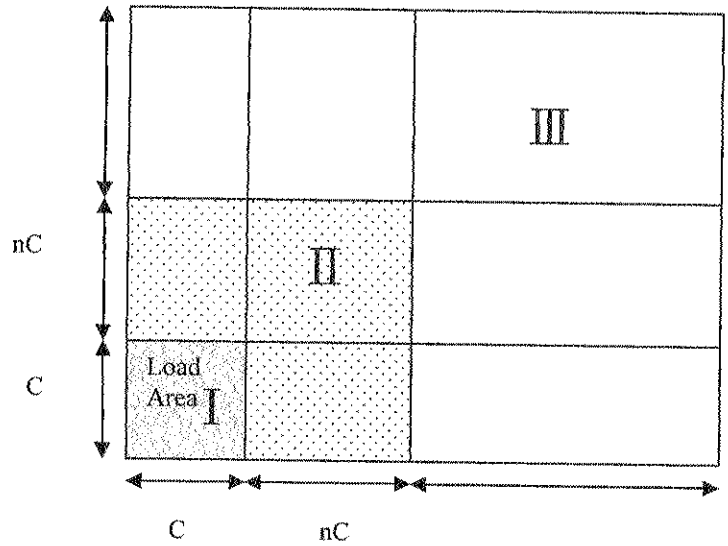

Figure 1: Illustration of Horizontal Mesh Generation Zones

3.2. Deflection convergence characteristics

A single finite slab resting on a Winkler foundation under edge loading conditions with the following input parameters: finite slab length L=5.00m (197 in.), slab width W=5.00m (197in.), E=8.27GPa (1.2Mpsi), h=21.6cm (8.5in.), k=27MN/m^3 (100pci), tire pressure p=620kPa (90psi), μ=0.15, P=10kN (2,250lbs) was chosen for the horizontal mesh fineness study. According to the principles of dimensional analysis, this is equivalent to a pavement having a/ℓ=0.1, L/ℓ=7, W/ℓ=7, and h/a=3 to be discussed later. For higher accuracy consideration, same horizontal mesh fineness of up to 10 for Zone I and Zone II was considered, in which the length of Zone II was set to 8 times the length of the loaded area (C). The slab thickness was sub-divided into up to 4 sub-layers for vertical mesh fineness study. The deflection convergence characteristics of various element types were investigated. The resulting deflections are generally in the following descending order: ABAQUS 3-D solid elements, 2-D shell elements, ILLI-SLAB element, and Westergaard solutions. The element types S8R, S8R5, and S9R5 resulted in very close deflection solutions. For 4-node shell elements, the deflections are in the following order: S4R5<S4<S4R when coarser mesh was used. The convergence characteristics of 8-node and 9-node elements are more effective than 4-node elements; and their deflections are generally slightly higher than 4-node element's deflections. For 3-D solid elements, using vertical mesh fineness of 1 (or 1-layer) was proved inadequate. By increasing horizontal and vertical mesh fineness, the resulting deflections of 8-node solid elements are very close to 20-node and 27-node elements. Generally speaking, the deflections of all 2-D shell and 3-D solid elements tend to increase to convergence when a finer horizontal mesh is used. Nevertheless, the deflections of C3D20, C3D20R, and C3D27 tend to increase to convergence whereas the deflections of C3D8, C3D8R, and C3D27R tend to decrease to convergence for finer vertical mesh, i.e., sub-divided into more layers. To achieve high accuracy and computation efficiency, it was recommended that element types

C3D20 or C3D27 with a horizontal mesh fineness of 3 and a vertical mesh fineness of 3 be selected for further analysis.

3.3. Stress convergence characteristics

Similarly, the stress convergence characteristics of various element types were subsequently investigated. The stresses of 8-node and 9-node shell elements tend to decrease to convergence whereas the stresses of 4-node shell elements increase to convergence when finer horizontal mesh was used. The element types S8R5 and S9R5 resulted in very close stress solutions. Using vertical mesh fineness of 1-layer was proved inadequate and should be avoided for 3-D solid elements.

Regardless of increasing horizontal and vertical mesh fineness, the resulting stresses of 8-node solid elements are very different from 20-node and 27-node elements. The edge stresses of element types C3D20 and C3D27 increase to convergence at a faster rate than any other 3-D solid elements when finer vertical mesh was used. The solid elements with reduced integration resulted in stress reduction of approximate 1% when compared to those without reduced integration. The stresses of 20-node elements were approximate 2% lower than 27-point elements when coarser mesh was used. The execution time of 20-point elements is approximate 60% of that of 27-point elements.

Thus, the above recommendation for selecting element types C3D20 or C3D27 with a horizontal mesh fineness of 3 and a vertical mesh fineness of 3 remains unchanged to achieve high accuracy and computation efficiency. Figure 2 and Figure 3 display the edge stress convergence characteristics of 2-D shell and 3-D solid elements, respectively. In which, stress ratio is defined as the ratio of the resulting FE stresses to the corresponding Westergaard solutions; horizontal mesh fineness=1~10; and vertical mesh fineness=1~4.

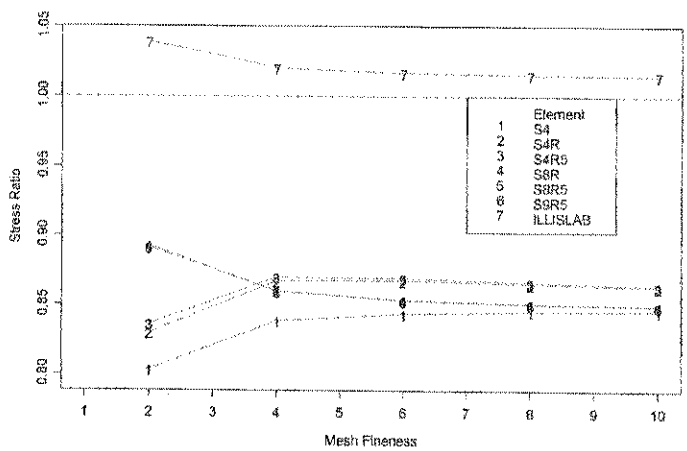

Figure 2: Edge Stress Convergence Characteristics (2-D Shell Elements)

3.4. Convergence characteristics due to different slab thicknesses and load sizes

The following 8 pavement-loading systems were chosen to investigate the effects of different slab thicknesses and load sizes to convergence characteristics: L/ℓ=7, W/ℓ=7; h/a=2, 4; and a/ℓ=0.05, 0.1, 0.2, 0.3. Element type C3D27 was chosen for the remaining analyses hereafter. The vertical or horizontal mesh fineness was set to 3 to study the effects of horizontal or vertical mesh fineness (up to 5) to the convergence characteristics of edge loading conditions.

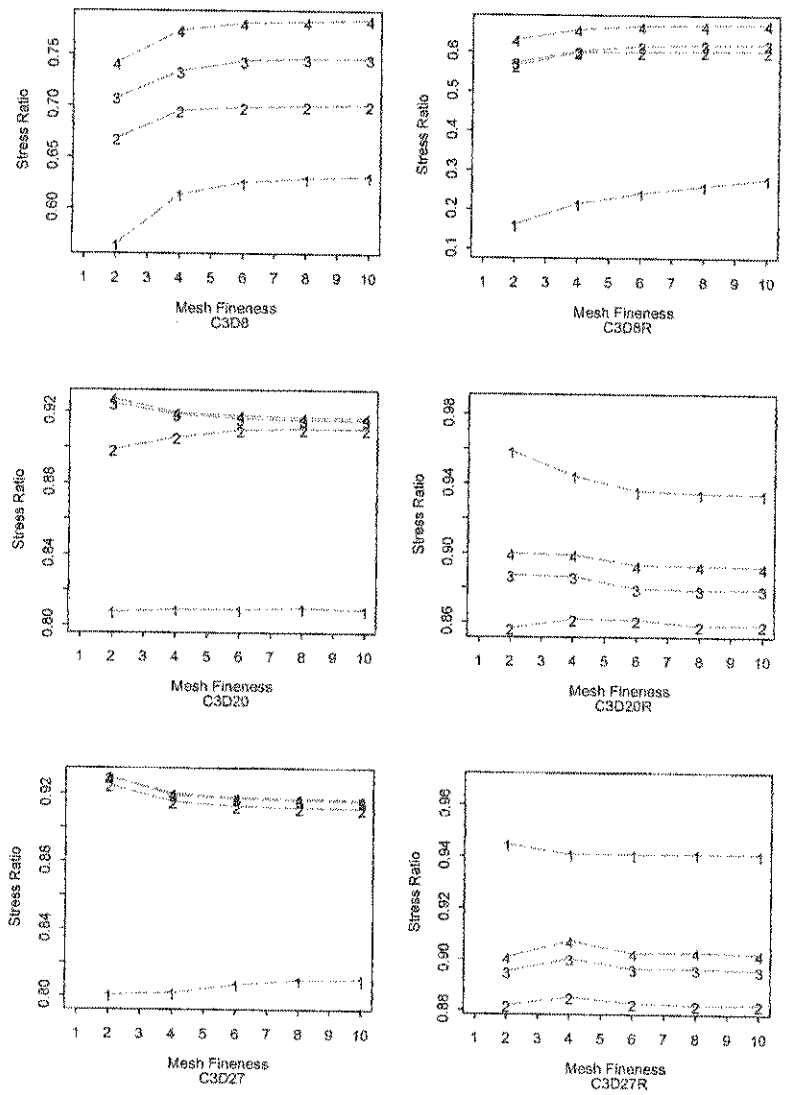

Figure 3: Edge Stress Convergence Characteristics (3-D Solid Elements)

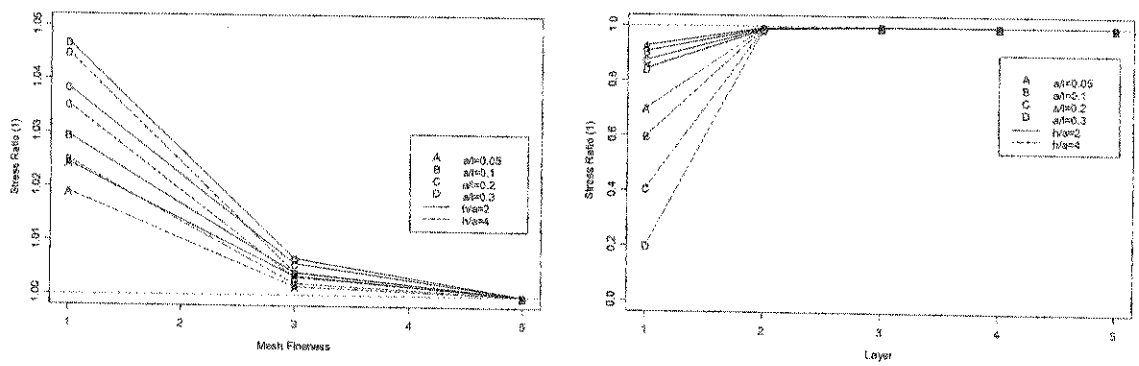

(a) Horizontal Mesh Fineness

(b) Vertical Mesh Fineness

Figure 4: Mesh Fineness Studies for Different Slab Thicknesses and Load Sizes

The deflections increase to convergence when finer horizontal mesh or finer vertical mesh is used. The deflections of a pavement with smaller slab thickness and load size (smaller h/a and a/ℓ) converge faster. Similarly, edge stress convergence patterns were investigated as shown in Figure 4. The edge stresses of C3D27 element decrease to convergence when finer horizontal mesh is used, whereas they increase to convergence when finer vertical mesh or more sub-layers are used. In which stress ratio (1) stands for the ratio of the resulting ABAQUS stress of any mesh fineness to that of the finest mesh used.
The effect of vertical mesh fineness to stress is higher than that of horizontal mesh fineness. The thicker the pavement (larger h/a), the more difficult the stresses will achieve convergence. The aforementioned recommendation of selecting a horizontal mesh fineness of 3 and a vertical mesh fineness of 3 is adequate to achieve good convergence and computation efficiency.

3.5. Determination of the length of neighborhood area

The length of neighborhood area (nC) selected for finer horizontal mesh was further investigated, in which n ranging from 1 to 8 was selected to study its effects on the results of FE computation accuracy. The pavement-loading system having a/ℓ=0.1, L/ℓ=7, W/ℓ=7, and h/a=3 previously described in Section 3.2 was re-analyzed here. All the aforementioned element types with a horizontal mesh fineness of 3 and a vertical mesh fineness of 3 were analyzed. The resulting FE deflections and stresses of any mesh fineness were compared to the corresponding ones with the finest mesh (or 8 times the length of the loaded area C). The deflections and stresses of ILLI-SLAB and 4-node elements were affected by the length of Zone II. However, the resulting deflections and stresses of 8-node and 9-node elements were identical when nC is greater than or equal to 2 times the length of the loaded area C. Regardless of different nC values selected, the resulting deflections and stresses of 20-node and 27-node solid elements are identical or almost identical. The differences in deflection due to the selection of nC are negligible. When nC is greater than or equal to 3 times C, the differences in the resulting stresses of 2-D shell elements are negligible. Thus, a value of 3 times C is recommended for all element types for consistency and conservative consideration.

4. IDENTIFICATION OF ADDITIONAL DIMENSIONLESS VARIABLE

According to previous literature, the following relationship has been identified and verified through many 2-D ILLI-SLAB studies for a constant Poisson's ratio (Ioannides, Thompson, and Barenberg, 1985; Ioannides and Salsilli-Murua, 1989; Salsilli-Murua, 1991; Lee, 1993):

$$\frac{\sigma h^2}{P}, \frac{\delta k \ell^2}{P} = f\left(\frac{a}{\ell}, \frac{L}{\ell}, \frac{W}{\ell}\right) \tag{3}$$

Extreme difficulties were encountered while using only these three dimensionless variables for 3-D FE (ABAQUS) analyses. Based on the principles of dimensional analysis, in addition to the normalized load radius (a/ℓ), the normalized finite slab length (L/ℓ), and the normalized finite slab width (W/ℓ), an additional dominating dimensionless variable (h/a) defined as the ratio of slab thickness (h) and load radius (a) was subsequently identified. The following relationship can be used to account for the theoretical differences of various 2-D shell and 3-D solid elements:

$$\frac{\sigma h^2}{P}, \frac{\delta k \ell^2}{P} = f\left(\frac{a}{\ell}, \frac{L}{\ell}, \frac{W}{\ell}, \frac{h}{a}\right) \tag{4}$$

While keeping the above four dimensionless variables constant and changing any other input parameters (a, h, ℓ, L, W, E, k, P), the resulting dimensionless 3-D FE stresses ($\sigma h^2/P$) and

deflections ($\delta k\ell^2/P$) remained constant. This relationship was numerically verified with the selected element type C3D27 as well as the aforementioned 2-D shell element types (Wu, 2003). Some results for edge loading analysis are summarized in Table 1 for the identification of an additional dimensionless variable.

Table 1: Identification and Verification of Dimensionless Variables (Edge Loading)

h/a	a/ℓ	L/ℓ	W/ℓ	C	a	h	ℓ	L	W	E	k	p	P	σ	δ	σh^2/P	δ*k*ℓ^2/P
				cm	cm	cm	cm	m	m	GPa	MN/m^3	kPa	kN	kPa	mm		
3.0	0.1	2	2	12.7	7.2	21.5	71.7	1.43	1.43	13.78	44.1	482.3	7.8	403.8	0.3491	2.3983	1.0200
3.0	0.1	2	2	19.1	10.7	32.2	107.5	2.15	2.15	10.34	22.0	620.1	22.5	519.2	0.8977	2.3984	1.0199
3.0	0.1	2	2	19.1	10.7	32.2	107.5	2.15	2.15	13.78	29.4	551.2	20.0	461.5	0.5984	2.3984	1.0199
3.0	0.1	2	2	25.4	14.3	43.0	143.3	2.87	2.87	24.12	38.6	689.0	44.5	576.8	0.5700	2.3985	1.0200
3.0	0.1	2	2	25.4	14.3	43.0	143.3	2.87	2.87	31.01	49.6	1033.5	66.8	865.4	0.6650	2.3989	1.0200
3.0	0.1	2	2	31.8	17.9	53.7	179.1	3.58	3.58	20.67	26.4	895.7	90.4	749.6	1.0806	2.3976	1.0200
3.0	0.1	2	2	31.8	17.9	53.7	179.1	3.58	3.58	27.56	35.2	413.4	41.7	346.1	0.3740	2.3983	1.0199
3.0	0.1	2	2	38.1	21.5	64.5	215.0	4.30	4.30	13.78	14.7	826.8	120.2	692.4	1.7954	2.3993	1.0199
3.0	0.1	2	2	38.1	21.5	64.5	215.0	4.30	4.30	41.34	44.1	620.1	90.1	519.1	0.4488	2.3982	1.0199
3.0	0.1	2	2	38.1	21.5	64.5	215.0	4.30	4.30	27.56	29.4	689.0	100.1	576.8	0.7481	2.3985	1.0200
6.0	0.2	3	3	12.7	7.2	43.0	35.8	1.07	1.07	13.78	5639.9	482.3	7.8	58.9	0.0119	1.3991	1.1148
6.0	0.2	3	3	19.1	10.7	64.5	53.7	1.61	1.61	10.34	2820.0	620.1	22.5	75.7	0.0307	1.3993	1.1147
6.0	0.2	3	3	19.1	10.7	64.5	53.7	1.61	1.61	13.78	3760.0	551.2	20.0	67.3	0.0204	1.3994	1.1147
6.0	0.2	3	3	25.4	14.3	86.0	71.7	2.15	2.15	24.12	4934.9	689.0	44.5	84.1	0.0195	1.3991	1.1147
6.0	0.2	3	3	25.4	14.3	86.0	71.7	2.15	2.15	31.01	6344.9	1033.5	66.8	126.2	0.0227	1.3987	1.1147
6.0	0.2	3	3	31.8	17.9	107.5	89.6	2.69	2.69	20.67	3384.0	895.7	90.4	109.3	0.0369	1.3989	1.1148
6.0	0.2	3	3	31.8	17.9	107.5	89.6	2.69	2.69	27.56	4512.0	413.4	41.7	50.5	0.0128	1.3991	1.1147
6.0	0.2	3	3	38.1	21.5	129.0	107.5	3.22	3.22	13.78	1880.0	826.8	120.2	100.9	0.0613	1.3990	1.1147
6.0	0.2	3	3	38.1	21.5	129.0	107.5	3.22	3.22	41.34	5639.9	620.1	90.1	75.7	0.0153	1.3993	1.1147
6.0	0.2	3	3	38.1	21.5	129.0	107.5	3.22	3.22	27.56	3760.0	689.0	100.1	84.1	0.0255	1.3992	1.1147

Note: 1 in.=2.54cm, 1 psi=6.89kPa, and 1 pci = 0.27MN/m^3, 1 kip=4.45 kN.

The identification of the aforementioned parameter (h/a) was originally inspired by the solutions and charts of Burmister's layered theory for a two-layer system and a three-layer system (Burmister, 1943, 1945; Huang, 1993). A more in-depth literature survey conducted after the completion of the study by Wu (2003) also indicated that analytical solutions derived for thick elastic plates are governed by the ratio of a circular load radius, a, to the thickness of the slab, h (Shi and Yao, 1989; Van Cauwelaert, 1990; Ioannides and Khazanovich, 1994; Khazanovich and Ioannides,1995). In which, different a/h ratios were used to compute the maximum bending stress at the bottom of the slab, σ, in terms of the percent of the applied pressure, p. The conventional Westergaard's ordinary theory solution results in an overestimate in the bending stress. The correction introduced by Westergaard's special theory results in bending stress reduction, bringing it in line with Burmister's layered solutions (Ioannides and Khazanovich, 1994).

5. DEVELOPMENT OF DATABASES AND PREDICTION MODELS

An automated analysis program was developed using the Visual Basic software package to automatically construct FE models, generate the input files, conduct the runs, as well as summarize the results. This program was also capable of assisting in conducting all the aforementioned analyses through the selection of various 2-D shell and 3-D solid elements, horizontal and vertical mesh fineness, and the length of the Zone II.

A series of 3-D FE factorial runs was conducted for a single slab resting on a Winkler foundation with edge loading conditions based on the following dimensionless parameters: L/ℓ =2~7 (step by 1); $W/\ell = L/\ell$; a/ℓ =0.05, 0.1~0.5 (step by 0.1); and h/a=0.5~6 (step by 0.5). These ranges were carefully selected to cover a very wide range of highway and airfield rigid pavement conditions. Separate deflection and stress databases were created using element type C3D27 with a horizontal mesh fineness of 3, a vertical mesh fineness of 3, and the same finer mesh extended to 3 times the length of loaded area (C).

Deflection ratios and stress ratios defined as the ratio of 3-D FE results to Westergaard solutions were calculated while assuming the normalized slab width W/ℓ equals to L/ℓ, i.e.,

square slabs. Note that Westergaard's closed-from solutions only serve as benchmarks herein instead of "exact solutions" since the solutions are based on the simplification which ignores plate compressibility and shear deformation. Since the resulting deflection ratios always had a value greater than one, their reciprocals or adjustment factors (R) will range from 0 to 1. The very high deflection ratios occurred when a thicker pavement (larger h/a) or a larger load size (larger a/ℓ) was analyzed. Similarly, the resulting edge stress ratios ranged from 0.25 to 1.03. To illustrate possible applications of these databases, the following predictive model was developed for critical edge stress estimation using projection pursuit regression technique (Lee and Darter, 1994; Friedman and Stuetzle, 1981):

$$R_{3D} = \frac{\sigma_{3DFEM}}{\sigma_{we}} = f\left(\frac{a}{\ell}, \frac{L}{\ell}, \frac{h}{a}\right)$$

$$R_{3D} = 0.69149 + 0.259\ \Phi_1 + 0.03318\ \Phi_2 \tag{5}$$

$$\Phi_1 = \begin{cases} 1.578 + 6.013(A1) + 2.673(A1)^2 + 0.208(A1)^3 & \text{if } (A1) \le -0.25 \\ 1.076 + 1.812(A1) - 5.796(A1)^2 + 4.942(A1)^3 & \text{if } (A1) > -0.25 \end{cases}$$

$$\Phi_2 = \begin{cases} -2.649 + 78.163(A2) + 381.681(A2)^2 - 15547.789(A2)^3 & \text{if } (A2) \le 0.05 \\ -0.927 + 39.165(A2) - 321.743(A2)^2 - 877.365(A2)^3 & \text{if } (A2) > 0.05 \end{cases} \tag{6}$$

$$A1 = 0.36539x1 - 0.01440x2 - 0.04566x3 + 0.85799x4 - 0.35545x5 + 0.04123x6$$

$$A2 = 0.23203x1 + 0.01107x2 - 0.00427x3 - 0.97246x4 + 0.01825x5 - 0.00230x6$$

$$X = [x1, x2, x3, x4, x5, x6] = \left[\frac{a}{\ell}, \frac{L}{\ell}, \frac{h}{a}, \frac{a}{\ell} / \frac{L}{\ell}, \frac{a}{\ell} \times \frac{h}{a}, \frac{L}{\ell} / \frac{h}{a}\right]$$

Statistics: N=432, R^2=0.9988, SEE=0.008745

Limits: $0.05 \le a/\ell \le 0.5, 0.5 \le h/a \le 6.0, 2 \le L/\ell \le 7, W/\ell = L/\ell$

In which, N stands for the number of observations; R^2 is the coefficient of determination; SEE is the standard error of estimation. A scatter plot matrix of the data also indicated that this additional variable (h/a) is the most influential parameter among those dominating dimensionless parameters.

6. IMPLICATIONS TO FUTURE APPLICATIONS

Jointed concrete pavements consist of many single finite concrete slabs jointed by aggregate interlock, dowel bars, or tie bars. Traffic loading may be in the form of dual, tandem, or tridem axle. A widened outer lane may also shift the wheel loading away from Westergaard's critical loading locations. A tied concrete shoulder and a second bonded or unbonded layer may also result in different degrees of stress reduction. The effect of a linear or nonlinear temperature differential may alter the magnitude of critical stresses. Thorough treatments of various combinations of all such conditions are extremely challenging due to the complexity and vast amount of required computation time in 3-D FE analysis.

A possible but aggressive approach to this problem may be to make the best use of the existing 2-D FE research findings (Lee, 1999), and strive to integrate them with new 3-D FE results. Since, adjustment factors are simply defined as a proportional relationship of the results of a specified condition to those of an ideal condition. Thus, the following tentative stress predictive model may be used to estimate critical edge stress in a mechanistic design procedure, though its applicability should be further verified and adjusted:

$$\sigma_e = \left(\sigma_{we} * R_{3D} * R_G * R_S * R_O * R_M + R_T * \sigma_c\right) \tag{7}$$

Where, R_{3D} stands for an adjustment factor for finite slab length and width using 3D FE analysis. The remaining adjustment factors still remain as the same existing 2-D FE findings,

in which R_G is the adjustment factor for different gear configurations including dual-wheel, tandem axle, and tridem axle; R_S the adjustment factor for a tied concrete shoulder; R_O is the adjustment factor for a widened outer lane; R_M is the adjustment factor for a bonded/unbonded second layer; and R_T is the adjustment factor for the combined effect of loading plus daytime curling. σ_c is the Westergaard/ Bradbury edge curling solution, [FL^{-2}].

7. DISCUSSIONS AND CONCLUSIONS

In-depth parameter studies on 3-D ABAQUS finite element analysis of rigid pavements under edge loading conditions were conducted. As expected, the resulting deflections are generally in the following descending order: ABAQUS 3-D solid elements, 2-D shell elements, ILLI-SLAB element, and Westergaard solutions. Generally speaking, with the exception of C3D8, C3D8R, and C3D27R elements, the deflections of all 2-D shell and 3-D solid elements tend to increase to convergence when a finer horizontal and or vertical mesh is used. The stresses of 8-node and 9-node shell elements tend to decrease to convergence whereas the stresses of 4-node shell elements increase to convergence with finer horizontal mesh. The stresses of element types C3D20 and C3D27 increase to convergence at a faster rate than any other 3-D solid elements when finer vertical mesh was used.

The vertical mesh fineness was defined as the number of evenly divided slab layers for simplicity and practical model building concern in this study. Using vertical mesh fineness of 1 (or 1-layer) was proved inadequate and should be avoided for 3-D solid elements. To achieve high accuracy and computation efficiency, element type C3D27, a horizontal mesh fineness of 3, a vertical mesh fineness of 3, and a value of 3 times C as the length of neighborhood area are recommended and adopted in this study. This recommendation for vertical mesh fineness is also in good agreements with Hammons' study (1998) that "at least three (evenly divided) elements through the slab thickness is likely a good choice ..." Nevertheless, attempt to maintain the element aspect ratios in all three dimensions to reasonable values may be too cumbersome especially for a small wheel load area and/or small horizontal mesh length.

An additional dominating dimensionless variable (h/a) was identified and verified to have a substantial influence on ABAQUS runs using either 2-D shell or 3-D solid elements. Separate stress and deflection databases were created using all dominating dimensionless parameters. An example critical stress predictive model in terms of adjustment factors was presented to illustrate their possible applications.

ACKNOWLEDGEMENTS

This study was sponsored by the National Science Council, Taiwan. This paper presents excerpts from Mr. Hsin-Ta Wu's M.S. thesis (Wu, 2003). Mr. Shao-Tang Yen consistently provided fruitful technical assistance in 3-D ABAQUS analyses. Dr. Chen-Ming Kuo and Dr. Ping-Sien Lin are gratefully acknowledged for their helpful guidance and recommendations.

REFERENCES

Brill, D. R. (1998). *Development of Advanced Computational Models for Airport Pavement Design*. DOT/FAA/AR-97/47.

Burmister, D. M. (1943). "The Theory of Stresses and Displacements in Layered Systems and Applications to the Design of Airport Runways," *Proceedings, Highway Research Board*, Vol. 23, pp. 126-144.

Burmister, D. M. (1945). "The General Theory of Stresses and Displacements in Layered Soil

Systems," *Journal of Applied Physics*, Vol. 16, pp. 84-94, 126-127, 296-302.
Friedman, J. H. and W. Stuetzle (1981). "Projection Pursuit Regression," *Journal of the American Statistical Association*, Vol. 76, pp. 817-823.
Hammons, M. I. (1998). *Advanced Pavement Design: Finite Element Modeling for Rigid Pavement Joints*. Report II: Model Development, DOT/FAA/AR-97-7.
Hibbitt, Karlsson, and Sorensen (2000). *ABAQUS/Standard User's Manual*. Vol. I & II.
Huang, Y. H. (1993). *Pavement Analysis and Design*. Prentice-Hall Inc.
Ioannides, A. M. (1984). Analysis of Slabs-on-Grade for a Variety of Loading and Support Conditions. Ph.D. Dissertation, University of Illinois, Urbana, Illinois.
Ioannides, A. M. and J. P. Donnelly (1988). "Three-Dimensional Analysis of Slab on Stress-Dependent Foundation." In *Transportation Research Record 1196*, Transportation Research Board, National Research Council, Washington, D.C., pp. 72-84.
Ioannides, A. M. and L. Khazanovich (1994). "Analytical and Numerical Methods for Multi-Layered Concrete Pavements," *Proceedings*, 3rd International Workshop on the Theoretical Design of Evaluation of Concrete Pavements, September 29-30, Krumbach, Austria, pp. 113-121.
Ioannides, A. M., M. R. Thompson, and E. J. Barenberg (1985). "Westergaard Solution Reconsidered," *Transportation Research Record* 1043, pp. 12-23.
Ioannides, A. M. and R. A. Salsilli-Murua (1989). "Temperature Curling in Rigid Pavements: An Application of Dimensional Analysis." In *Transportation Research Record* 1227, pp. 1-11.
Khazanovich, L. and A. M. Ioannides (1995). "DIPLOMAT: Analysis Program for Bituminous and Concrete Pavements." In *Transportation Research Record 1482*, pp. 52-60.
Kim., J., and K. Hjelmstad (2000). *Three-Dimensional Finite Element Analysis of Multi-Layered Systems: Comprehensive Nonlinear Analysis of Rigid Airport Pavement Systems*, Federal Aviation Administration DOT 95-C-001.
Korovesis, G. T. (1990). *Analysis of Slab-on-Grade Pavement Systems Subjected to Wheel and Temperature Loadings*. Ph.D. Dissertation, University of Illinois, Urbana, Illinois.
Kuo, C. M. (1994). *Three-Dimensional Finite Element Model for Analysis of Concrete Pavement Support*. Ph.D. Dissertation, University of Illinois, Urbana, Illinois.
Lee, Y. H. (1993). *Development of Pavement Prediction Models*. Ph.D. Dissertation, University of Illinois, Urbana, Illinois.
Lee, Y. H., and M. I. Darter (1994). "New Predictive Modeling Techniques for Pavements," *Transportation Research Record* 1449, National Research Council, pp. 234-245.
Lee, Y. H. (1999). "TKUPAV: Stress Analysis and Thickness Design Program for Rigid Pavements," *Journal of Transportation Engineering*, Vol. 125, No. 4, ASCE, pp. 338-346.
Salsilli-Murua, R. A. (1991). *Calibrated Mechanistic Design Procedure for Jointed Plain Concrete Pavements*, Ph.D. Dissertation, University of Illinois, Urbana, Illinois.
Shi, X. and Z. Yao (1989). "Concrete Pavement Design Procedure for Container Terminals," *Proceedings*, 4th International Conference on Concrete Pavement Design and Rehabilitation, Purdue University, West Lafayette, Indiana, April 18-20, pp. 53-59.
Thompson, M. R., G. Navneet (1999). *Wheel Load Interaction: Critical Airport Pavement Responses*. FAA, DOT95-C-001, Final Report.
Van Cauwelaert, F. (1990). "Westergaard's Equations for Thick Elastic Plates," *Proceedings*, 2nd International Workshop on the Theoretical Design of Concrete Pavements, October 4-5, Sigüenza, Spain, pp. 165-175.
Wu, H.-T. (2003). *Parameter Analysis and Verification for Jointed Concrete Pavements*. M.S. Thesis, Tamkang University, Tamsui, Taiwan, January 2003. (In Chinese)